Am J Nucl Med Mol Imaging 2015;5(4):317-332
www.ajnmmi.us /ISSN:2160-8407/ajnmmi0008827

Review Article

Imaging radiation response in tumor and normal tissue

Marjan Rafat, Rehan Ali, Edward E Graves

Department of Radiation Oncology, Stanford University, Stanford, CA 94305, USA

Received April 6, 2015; Accepted May 8, 2015; Epub June 15, 2015; Published July 1, 2015

Abstract: Although X-ray computed tomography (CT) and magnetic resonance imaging (MRI) are the primary imaging modalities used in the clinic to monitor tumor response to radiation therapy, multi-modal molecular imaging may facilitate improved early and specific evaluation of this process. Fast and accurate imaging that can provide both quantitative and biological information is necessary to monitor treatment and ultimately to develop individualized treatment options for patients. A combination of molecular and anatomic information will allow for deeper insight into the mechanisms of tumor response, which will lead to more effective radiation treatments as well as improved anti-cancer drugs. Much progress has been made in nuclear medicine imaging probes and MRI techniques to achieve increased accuracy and the evaluation of relevant biomarkers of radiation response. This review will emphasize promising molecular imaging techniques that monitor various biological processes following radiotherapy, including metabolism, hypoxia, cell proliferation, and angiogenesis.

Keywords: Radiation therapy, molecular imaging, tumor microenvironment, tumor response, normal tissue response

Introduction

The goal of molecular imaging is to gain insight into biological functions and mechanisms by visualizing changes in physiological and cellular properties. Observing tissue response to cancer therapy may lead to the discovery of improved cancer treatments that may be tailored to an individual patient's needs. Conventional imaging techniques, including ultrasound (US) and X-ray computed tomography (CT), have been successful in providing an accurate visualization of anatomic features of tumors. Recent developments in molecular imaging probes and techniques, including biologically active PET tracers and specialized magnetic resonance imaging (MRI) pulse sequences, allow for the visualization of cellular properties and microenvironmental changes.

Radiotherapy has a long history in cancer treatment, stemming from Röntgen's discovery of the X-ray in 1895 [1]. Radiation therapy is used in the treatment of a wide range of cancers and is prescribed for over 50% of all cancer patients [2]. Since DNA damage is the mechanism by which ionizing radiation kills cells [3], exposure of normal tissue to radiation commonly limits the maximum deliverable dose and hence efficacy of this therapy through the induction of treatment-related toxicity [4]. The current clinical standard for evaluating response to treatment is to determine tumor size reduction on CT using a unidimensional measurement, termed Response Evaluation Criteria in Solid Tumors (RECIST) [5]. The RECIST criteria focus solely on tumor size reduction, which provides a limited view of treatment efficacy [6] and does not necessarily correlate with patient survival [7-9]. In addition to CT, other non-invasive imaging methods, including US and MRI, have been used to determine the response of tumors to radiation therapy by monitoring reduction in the size of the primary tumor after treatment [10]. Crucial information about the location of tumors and injury to surrounding areas can also be gained from these modalities. However, they are insensitive to the underlying biological changes that drive tissue response to radiation. Combining multiple modalities may improve outcomes not only by determining changes in tumor size but also by characterizing biological processes.

New clinical criteria have been proposed for assessing tumor volume changes that include biological information gained from PET imaging

Table 1. Methods for visualizing radiation response based on biological processes

Method	Tracer/Technique	Biological process	References
PET	FDG	Metabolism	[11, 13-21]
	FMISO	Hypoxia	[36, 37, 39, 41-47]
	FAZA	Hypoxia	[40, 48-50]
	EF5	Hypoxia	[38]
	^{60}Cu-ATSM	Hypoxia	[51, 52]
	FLT	Proliferation	[63-65]
	^{18}F-ISO	Proliferation	[69, 70]
	^{18}F-ML-10	Apoptosis	[90, 91]
	^{18}F-ICMT-11	Apoptosis	[84-89]
	^{18}F-galacto-RGD	Angiogenesis	[115-119]
MRI	^{1}H-MRSI	Metabolism	[22-27]
	^{13}C-MRSI	Metabolism	[28-31]
	BOLD	Hypoxia	[58]
	APT	Necrosis	[94, 95]
	DTI	Necrosis	[96, 97]
	DCE	Angiogenesis	[99, 102-106]
US	DCE	Angiogenesis	[110-114]

of glucose metabolism, called PET Response Criteria in Solid Tumors (PERCIST) [5]. The inclusion of PET imaging overcomes some limitations of anatomical imaging by allowing the assessment of early responses to treatment [11]. Whereas anatomical and structural changes have classically been the focus of tumor response to therapy, emerging imaging techniques provide crucial biological information at the molecular level. Molecular imaging provides a means to detect and predict biological responses to therapy (**Table 1**), allowing for the development of personalized treatment options. Being able to visualize radiation response in both tumors and normal tissues may aid in the determination of treatment efficacy (**Table 2**). Given the complex nature of the tumor microenvironment and its potential contribution to therapy response, molecular imaging can provide a means to visualize individual components of the microenvironment, including changes in the vasculature, immune response, and stroma [12]. This review highlights the current state of post-therapy biological response imaging and examines future directions for research in this area.

Metabolism

Following radiation therapy, tumor cell metabolic activity changes due to decreases in cell survival and proliferation. Imaging these metabolic changes is one avenue for measuring tumor response to treatment (**Figure 1A**). The most common radiotracer used in PET imaging is ^{18}F-fluoro-2-deoxyglucose (FDG), an analog of glucose incorporating a positron-emitting isotope of fluorine (^{18}F). Because glucose uptake is increased in most cancers, FDG-PET has been widely used to detect elevated glucose metabolism in both primary and metastatic tumors and to determine tumor response to therapy [11]. For example, FDG-PET has been used to monitor the response of locally advanced cervical cancer to chemoradiation [13-16]. FDG is also taken up by macrophages and inflammatory lesions [17]. This characteristic has been examined in patients with non-small cell lung cancer (NSCLC) to determine the response of normal lung and pleura to radiation by evaluating inflammatory changes based on FDG uptake [18]. FDG uptake in normal tissues within the radiation field was evaluated independently of tumor response using a qualitative scoring system (**Figure 1B**), and it was found that inflammatory changes in normal tissue stemming from radiation pneumonitis and pleuritis were positively correlated with the tumor metabolic response due to a potential relationship between the radiosensitivities of the tumor and normal tissue.

Despite its wide use in monitoring response to therapy [19-21], FDG lacks tumor specificity. As such, other means of monitoring tumor metabolism are being explored, including magnetic resonance spectroscopic imaging (MRSI), which allows for non-invasive, simultaneous acquisition of biochemical and anatomical properties [22]. Proton (^{1}H)-MRSI has been applied toward imaging gliomas in order to plan radiation treatments by distinguishing the abnormalities in metabolic properties of these tumors as compared to normal cerebral tissues [23-25]. ^{1}H-MRSI has also been shown to be effective in monitoring radiation response in brain tumors [22]. Characteristic changes in glioma-associated metabolites, including choline, creatine, lactate, and lipids, have been shown with ^{1}H-MRSI after radiotherapy, which could be indicative of patient response to treatment [26, 27]. Similar to PET imaging which

Table 2. Methods for determining normal tissue response following radiotherapy

Modality	Tissue	Readout	References
FDG-PET	Normal lung and pleura	Normal tissue uptake within radiation field	[18]
MRSI	Cerebral tissues	Normal metabolites	[23-25]
FLT-PET	Bone marrow	Hematopoietic cell uptake	[64]
DCE-MRI	White matter	K^{trans}	[106]

requires the injection of an exogenous probe, ^{13}C-MRSI uses hyperpolarized agents to increase the detection sensitivity of injected ^{13}C labeled molecules by greater than 10,000 fold [28]. ^{13}C-labeled molecules such as [1-^{13}C]-pyruvate [29], [1, 4-^{13}C]-fumarate [30], and $_{L}$-[5-^{13}C-4-2H_2]-glutamine [31] can be used for imaging metabolism, cell death, and cell proliferation, respectively. The first clinical trial using this technique detected elevated levels of ^{13}C-pyruvate in known areas of prostate cancer, showing its feasibility in examining tumor therapeutic response (**Figure 1C**) [32]. Monitoring changes in metabolic processes following radiation therapy is promising for detecting early treatment response in patients, however it is limited to observation of molecules that can be delivered and metabolized within the lifetime of hyperpolarization, typically 1-2 minutes [32].

Hypoxia

It has been established that hypoxia, or low oxygen, is an important factor in tumor response and resistance to therapy in many cancers [33]. Hypoxia influences tumor cell invasiveness, energy metabolism, gene expression, and metastasis [34]. Visualizing hypoxic areas within tumors as well as changes in oxygen levels after treatment may allow optimized treatment selection, planning, and adjustment (**Figure 2A**). For example, hypoxia-specific radiotracers are being investigated to non-invasively monitor hypoxic tumor populations following treatment [35]. Due to their reduction under low oxygen tension and intracellular binding in hypoxic cells [34, 35], 2'-nitroimidazole-containing compounds, such as ^{18}F-fluoromisonidazole (FMISO), ^{18}F-fluoroazomycin arabinoside (FAZA), and 2-(2-nitro-1*H*-imidazol-1-yl)-*N*-(2, 2, 3, 3, 3-^{18}F-pentafluoropropyl)-acetamide (EF5), are being used to quantify hypoxia based on tumor-to-plasma or tumor-to-muscle uptake ratios (T/M) [36-38]. These hypoxia markers exhibit similar signal-to-noise ratios (SNR): in head and neck cancer, for example, T/M ratios range from 1.1-3.2 for EF5 [38] to 1.1-3.0 for FMISO [39], and 1.6-2.4 for FAZA [40]. The widely-used PET tracer FMISO has been utilized to image and quantify hypoxic areas in many types of tumors, including lung, head and neck, and prostate [41-43]. A clinical trial of head and neck cancer patients used FMISO imaging before and after radiotherapy to define hypoxia kinetics over the course of treatment [44]. Another clinical trial conducted in patients with head and neck, gastrointestinal, lung, and uterine cancers successfully showed the feasibility of using FMISO to monitor the reoxygenation of hypoxic areas following radiotherapy [45]. The use of FMISO as a universal hypoxia marker is limited by contradictory results with respect to the correlation of FMISO uptake and hypoxia markers in various tumor types [46, 47], so FAZA is being evaluated as an additional tracer for detecting hypoxia [48]. FAZA has been used to image hypoxia in lung, head and neck, blood, and brain tumors [49]. In NSCLC patients, FAZA was used to monitor changes in hypoxia following chemoradiation. Despite limitations in the number of patients in the study, results indicated that therapy likely decreased tumor cell survival and improved reoxygenation of intratumoral regions [50].

PET imaging with copper-60 diacetyl-bis (*N* 4-methylthiosemicarbazone) (^{60}Cu-ATSM) is also being evaluated to improve upon the lower SNR of the previously mentioned hypoxia markers. T/M ratios between 3.0-3.5 have been defined in patients with NSCLC and cervical cancer [51, 52]. In both cases, it was found that uptake of ^{60}Cu-ATSM was variable based on the extent of hypoxia within tumors and that a decrease in T/M ratios correlated to patients who had responded to therapy. However, this technique suffers from time and tumor dependent variation in uptake and retention, which limits its use as a general hypoxia marker [53, 54].

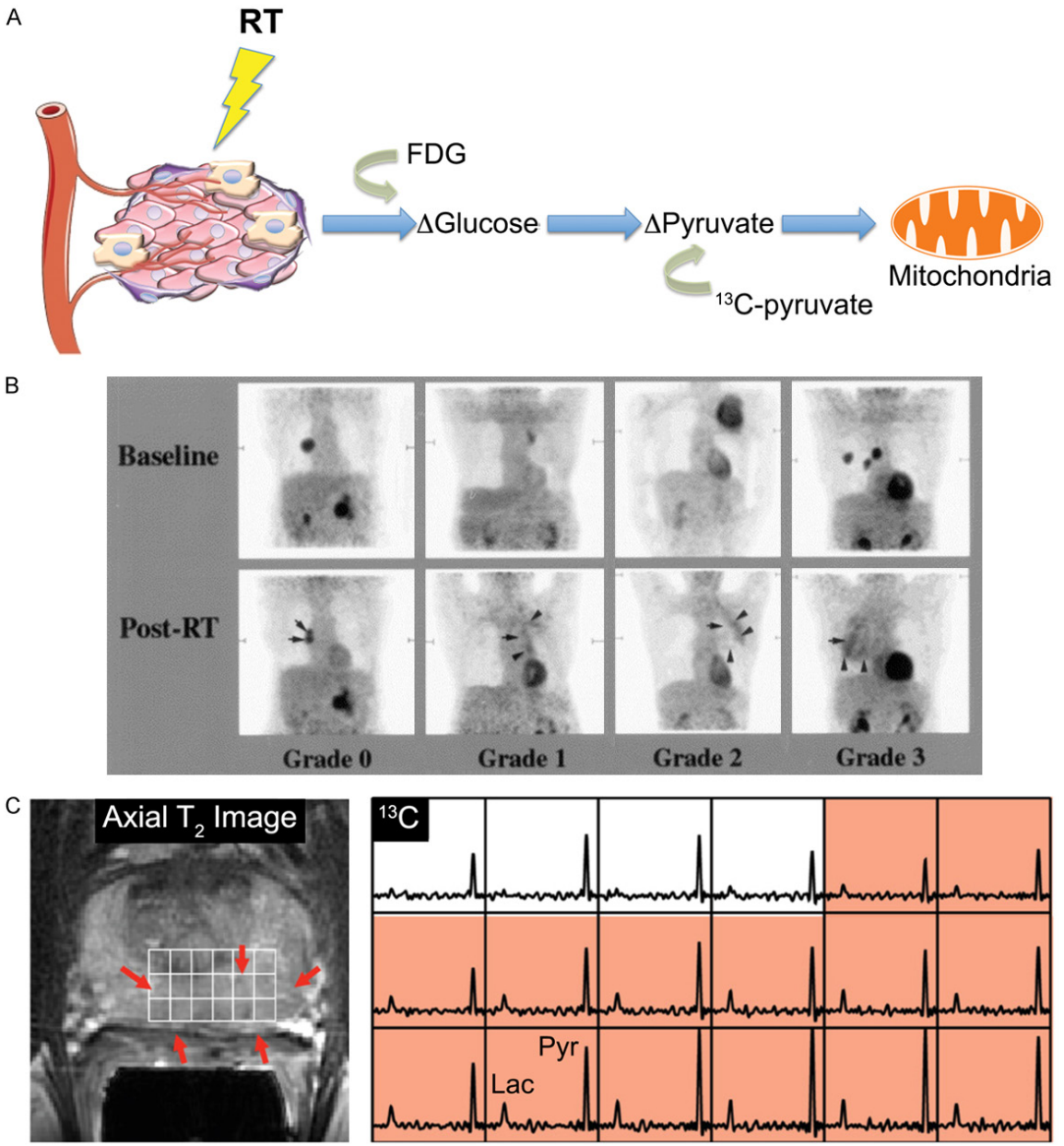

Figure 1. Imaging metabolism. A. The complex tumor microenvironment, consisting of tumor cells, vasculature, stromal cells, and immune cells, plays a critical role in response to therapy. Techniques such as FDG-PET that use glucose analogs to observe cellular uptake or ^{1}H or ^{13}C MRI that monitor metabolites can evaluate metabolic changes in the tumor microenvironment following radiotherapy (RT). B. FDG-PET scans performed in 4 different patients with NSCLC before (Baseline) and 6-12 weeks after radiotherapy (Post-RT) are shown. Horizontal arrows highlight the original tumor site, oblique arrows designate a new tumor site, oblique arrowheads show pleural reaction, and vertical arrowheads indicate parenchymal lung changes. A qualitative scoring system was devised to evaluate normal tissue FDG uptake for the determination of radiation-induced changes in inflammation. Grade 0 shows no normal tissue abnormalities within the treatment volume. Grade 1 denotes activity in the pleural reflections and soft tissues without parenchymal lung changes. Grade 2 indicates increased parenchymal uptake of equal or lower intensity than normal soft tissues while Grade 3 shows uptake in the right lung parenchyma of higher intensity than surrounding normal soft tissues. Reprinted with permission from [18]. C. ^{13}C-MRSI study in prostate cancer patient who received 0.43 mL/kg of hyperpolarized [1-^{13}C]pyruvate. T_2-weighted image through the malignant region (left) with corresponding ^{13}C-MRSI spectral array (right). Pink shading represents tumor. Lac = lactate; Pyr = pyruvate. Adapted from [32].

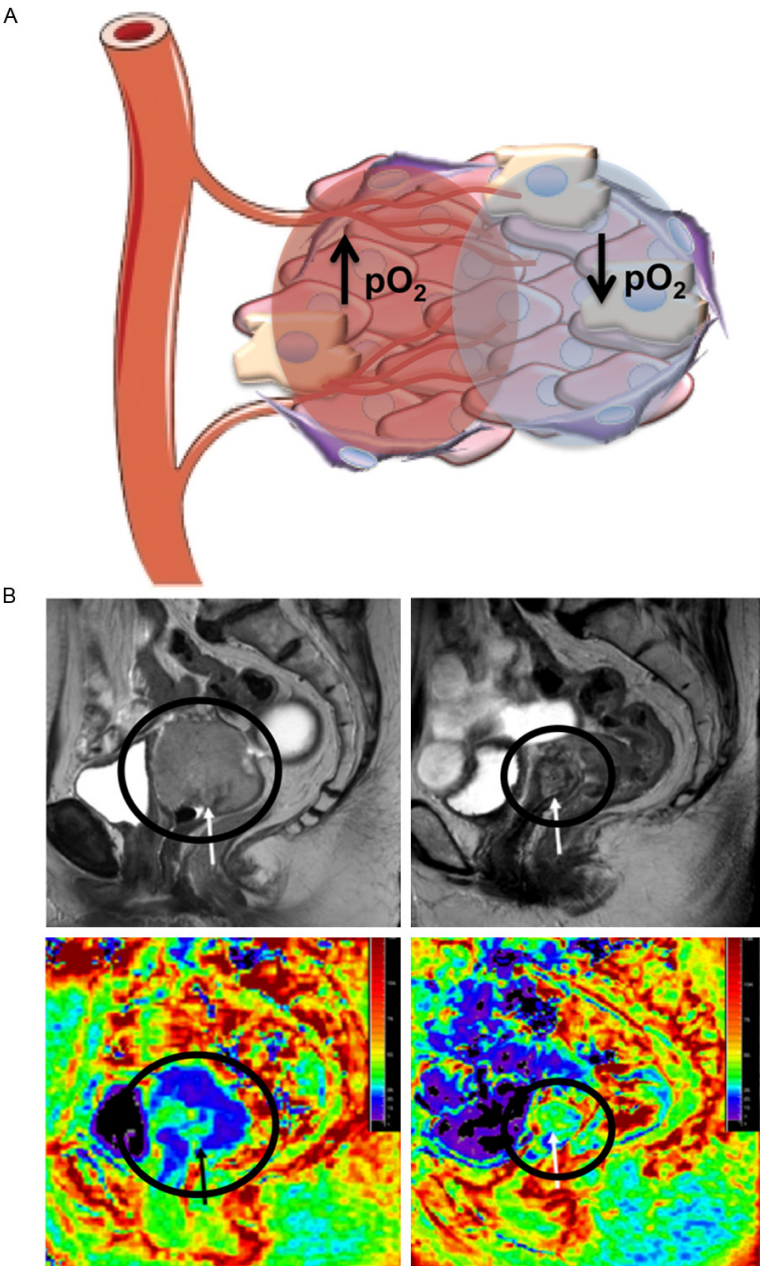

Figure 2. Hypoxia imaging. A. The tumor microenvironment exhibits heterogeneous levels of oxygenation, which can vary based on proximity to the vasculature: higher oxygen concentrations near vessels (red circle) and lower concentrations at greater distances (blue circle). Areas of hypoxia are resistant to radiotherapy. PET and MRI methods to image hypoxia levels before and after treatment are being explored. B. T2w and BOLD R2* MRI images of a patient with advanced cervical cancer undergoing concurrent chemoradiotherapy (left panels, before therapy; right panels, 1 month after therapy). T_2-weighted imaging (top panels) shows the size decrease of a cervical tumor (arrows, circles) following treatment. Color-coded R_2^* maps (bottom panels) demonstrate increases in R_2^* values post-therapy. Reprinted with permission from [58].

As an alternative to using PET, blood oxygenation level-dependent (BOLD) MRI is being used to assess tumor hypoxia in patients [55, 56]. BOLD MRI utilizes paramagnetic deoxyhemoglobin as an endogenous hypoxia marker, as the deoxyhemoglobin blood concentration alters the transverse relaxation rate R_2^* (1/T_2^*) and can indicate the oxygenation status of tissues adjacent to perfused microvessels [57]. In a clinical study of cervical cancer patients pre- and post-chemoradiation therapy, it was found that R_2^* and consequently tumor hypoxia increased following treatment, potentially indicating therapeutic efficacy through decreases in vascular permeability and blood flow (**Figure 2B**) [58]. In addition, no changes in the normal uterine myometrium before and after treatment were detected. Although there are limitations in correlating BOLD signal intensity to absolute pO_2 levels in tumors [59], recent pre-clinical work in rat prostate tumor models has combined T_2^*-weighted BOLD and T_1-weighted tissue oxygen level-dependent MRI to provide complementary evaluations of tumor oxygenation to better evaluate radiation response [60], which should be further validated in clinical studies.

Cell proliferation

Monitoring cell proliferation is an additional method of determining the success of cancer therapies: a decrease in proliferation can be attributed to the killing of rapidly proliferating cancer cells (**Figure 3A**).^{18}F-fluoro-3'-deoxythymidine (FLT), a thymidine analog, is being used to detect cell proliferation kinetics through phosphorylation by thymidine kinase 1, an enzyme involved in

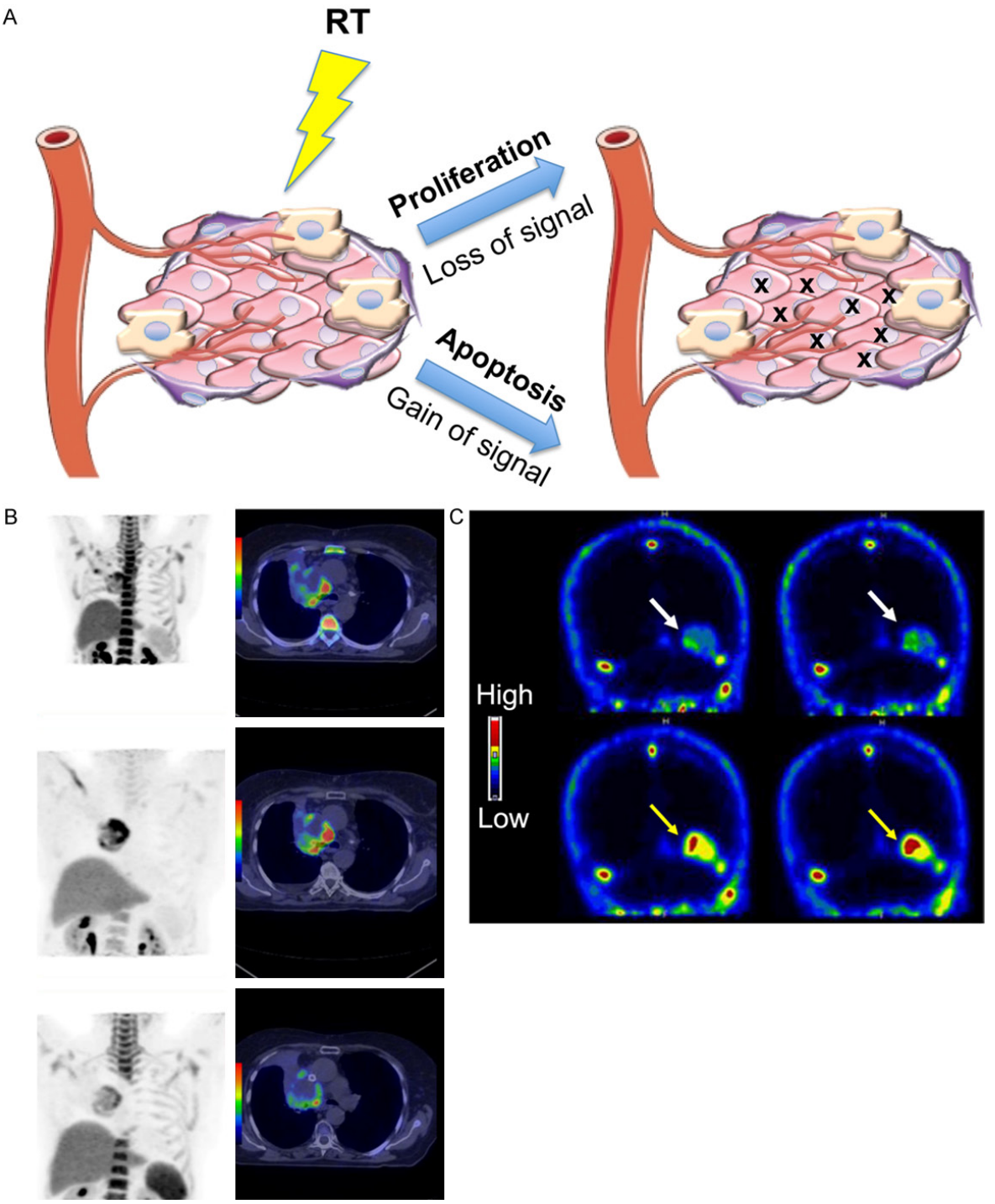

Figure 3. Cell proliferation and apoptosis imaging. A. Radiotherapy induces cell death in the tumor microenvironment, which can be monitored by PET either through the loss of cell proliferation or the increase in apoptosis. Tracers such as FLT and ^{18}F-ISO can be used to visualize decreases in cell proliferation while ^{18}F-ICMT-11 and ^{18}F-ML-10 have been used in the clinic to monitor apoptosis. B. FLT uptake in patients with NSCLC. Coronal ^{18}F-FLT PET (right panels) and transverse ^{18}F-FLT PET/CT (left panels) show baseline (top), 2 week (middle), and 4 week (bottom) response during chemo-RT. A reduction in proliferation was shown within 4 weeks of treatment. Adapted from [65]. C. Visualization of the effect of whole brain RT in two patients with brain metastases. White arrows show baseline ^{18}F-ML-10 uptake and yellow arrows indicate response after 10 fractions of RT. Uptake increased following RT, indicating induced apoptosis. Adapted from [90].

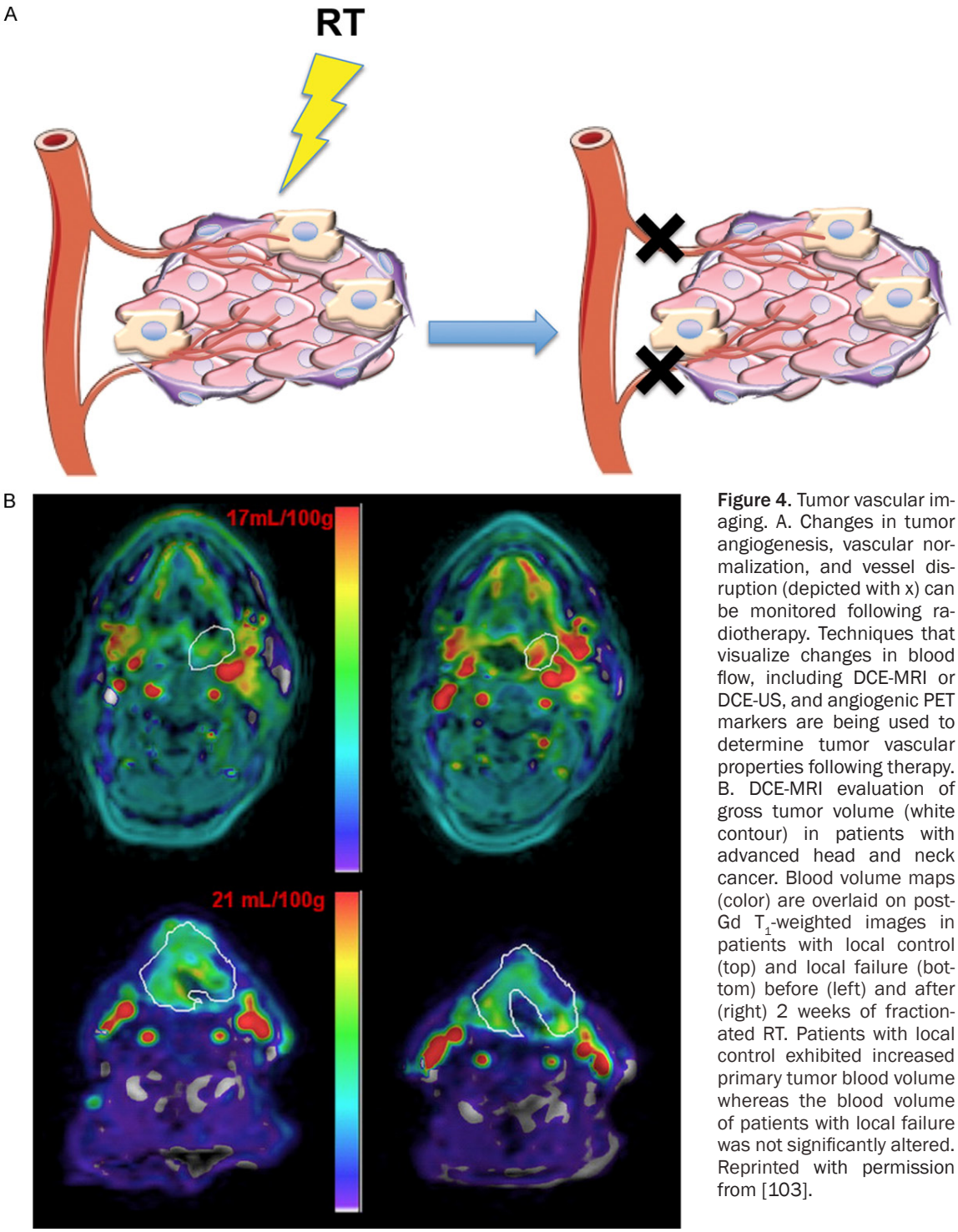

Figure 4. Tumor vascular imaging. A. Changes in tumor angiogenesis, vascular normalization, and vessel disruption (depicted with x) can be monitored following radiotherapy. Techniques that visualize changes in blood flow, including DCE-MRI or DCE-US, and angiogenic PET markers are being used to determine tumor vascular properties following therapy. B. DCE-MRI evaluation of gross tumor volume (white contour) in patients with advanced head and neck cancer. Blood volume maps (color) are overlaid on post-Gd T_1-weighted images in patients with local control (top) and local failure (bottom) before (left) and after (right) 2 weeks of fractionated RT. Patients with local control exhibited increased primary tumor blood volume whereas the blood volume of patients with local failure was not significantly altered. Reprinted with permission from [103].

the pyrimidine salvage pathway of DNA synthesis that has 3-4 times higher activity in malignant cells compared to benign cells [61, 62]. Recent studies have evaluated the use of FLT-PET to image radiation response in patients with head and neck cancer or NSCLC over the course of chemo-radiotherapy regimens [63-65]. In patients with head and neck cancer, FLT uptake in tumors significantly decreased in the first 4 weeks of therapy but remained the same in the surrounding normal tissues [63]. Patients with NSCLC exhibited heterogeneous patterns of tracer uptake and proliferation within individual tumors throughout the study, which

could be used to alter treatments based on individual responses [64]. A phase II trial confirmed that FLT-PET can be used to monitor early changes in cell proliferation as a response therapy in NSCLC patients (**Figure 3B**) [65]. The group also examined the proliferative response in the surrounding normal bone marrow [64]. A reduction of tracer uptake was observed in all cases, suggesting a decrease in the number of proliferating bone marrow cells. These findings illustrate the potential of monitoring cell proliferation to determine the extent of normal tissue damage after treatment.

Assessing proliferation based solely on FLT, or any thymidine analog uptake, is not feasible because these molecules accumulate as a function of the thymidine salvage pathway but do not necessarily reflect proliferation through the *de novo* thymidine pathway. They will therefore underestimate proliferation due to their inability to distinguish between proliferative cells in the G1, G2, and M phases and quiescent cells [66, 67]. Other tracers are being developed that can determine proliferative status more accurately, including ligands for the sigma-2-receptor, a validated cell proliferation biomarker [68]. One such proliferation tracer, N-(4-(6, 7-dimethoxy-3, 4-dihydroisoquinolin-2(1H)-yl)butyl)-2-(2-^{18}F-fluoroethoxy)-5-methylbenzamide (^{18}F-ISO-1), was tested in a preliminary clinical trial for evaluation of its biodistribution and dosimetry, and it was found that the PET results correlated to Ki67 expression, a well-established marker of proliferation, in tumor biopsies [69]. Although ^{18}F-ISO-1 has been used to monitor response following chemotherapy in mouse mammary tumors [70], more studies are needed to assess how changes in uptake of this agent may report on response following radiotherapy in patients.

Apoptosis

The ability to evade apoptosis, or programmed cell death, is a defining characteristic of cancer cells [71]. The link between apoptosis and radiation response has been studied extensively but remains a controversial topic. By evaluating the proportion of cells undergoing apoptosis following irradiation, some studies suggest that apoptosis may play a significant role in the response of tumors to radiotherapy [72, 73]. However, studies by Brown and Attardi concluded that while there is evidence of apoptosis following radiation treatment, cell death through mitotic catastrophe is the predominant mode of cell death [74]. Apoptosis nonetheless continues to be a focus of radiation research; recent studies have reinforced the observation that apoptosis is induced by radiation in breast cancer while noting an inverse correlation between apoptosis and DNA damage [75]. Huang and colleagues have also demonstrated that caspase-3 may regulate other secreted factors that can stimulate the proliferation of neighboring cells after the induction of apoptosis by radiation [76]. Taken together, these observations indicate that apoptosis occurs in a subset of tumor cells following radiotherapy and monitoring tumor cell apoptosis may be a valuable method of determining tumor response to treatment [77-82].

Unlike the previously mentioned PET techniques targeting cell proliferation, metabolism, and hypoxia, imaging apoptosis after therapy would provide a positive contrast (an increase in signal) following a successful therapy (**Figure 3A**). Because activation of caspase-3 drives the degradation of DNA into fragments during apoptosis, it is widely used as a biomarker for apoptosis [83]. A radiolabeled isatin sulfonamide, ^{18}F-(*S*)-1-((1-(2-fluoroethyl)-1H-[1, 2, 3]-triazol-4-yl) methyl)-5-(2(2, 4-difluorophenoxymethyl)- pyrrolidine-1-sulfonyl) isatin (^{18}F-ICMT-11), has been identified as a caspase-3-specific PET tracer [84]. In pre-clinical models, ^{18}F-ICMT-11 had increased tumor retention in murine lymphoma xenografts, which corresponded to drug-induced apoptosis and indicated early response to treatment [85, 86]. The tracer is currently being tested in clinical trials and has been shown to be safe with a favorable dosimetry profile in healthy subjects [87]. Further studies regarding the specificity of the tracer *in vivo* need to be done given the potential for non-specific binding of the probe to other nucleophilic cysteine proteases, which could limit its use in the clinic [88, 89]. Another PET tracer, 2-(5-fluoro-pentyl)-2-methyl-malonic acid (^{18}F-ML-10), has been used to visualize apoptosis of brain metastatic cells in patients following whole-brain radiation therapy (**Figure 3C**) [90]. ^{18}F-ML-10 was shown to have high signal-to-background ratios (between 1.75 to 20.45) in tumors as compared to healthy brain tissue and a statistically significant correlation

to response as evaluated by MRI after radiotherapy. This apoptotic tracer also facilitated early detection of response to therapy. Another advantage of this tracer is the ability to distinguish between apoptotic and necrotic cells through the loss of signal upon cell membrane rupture [91].

Necrosis

Differentiating between necrosis and recurrent tumors after radiation has been a long-standing challenge in the treatment of brain tumors [92, 93]. New MRI techniques have emerged that exploit inherent biological properties, including amide proton transfer (APT) MRI, that can detect amide protons of low concentration proteins [94]. Since malignant gliomas have higher protein and peptide content than normal tissue, differentiation of glioma and radiation necrosis with molecular APT-MRI has been shown to be feasible in a pre-clinical model [95]. However, clinical validation is necessary to optimize these techniques for use in patients. In addition, diffusion tensor imaging (DTI) using MRI can measure 3D diffusion of water *in vivo*. This technique has been used to create apparent diffusion coefficient (ADC) maps in order to discriminate necrotic areas from glioma recurrence following radiotherapy [96]. DTI-MRI has also been coupled with ^{1}H-MRS to track brain injury as a result of nasopharyngeal carcinoma radiation therapy [97]. Distinguishing viable tumor cells from radiation-induced necrosis is crucial in predicting and monitoring tumor response to therapy.

Tumor vascularity

Angiogenesis and abnormal vasculature are known to play important roles in tumor metastasis and response to therapy [98]. Monitoring changes in tumor vascularity, angiogenesis, and vessel normalization is another method of evaluating radiation response (**Figure 4A**). Dynamic contrast-enhanced (DCE)-MRI is a functional technique that is capable of quantifying vascular perfusion, microvessel density, and permeability by evaluating changes in signal intensity over time [99]. DCE-MRI allows for the differentiation of tumors compared to normal tissues due to their marked differences in terms of interstitial volume and permeability [100, 101]. In rectal cancer, DCE-MRI showed differences in microvessel properties after radiotherapy [102]. DCE-MRI has also been used to assess differences in tumor blood volume in head and neck cancer following chemoradiotherapy (**Figure 4B**) [103]. The technique has also been used to analyze changes in tumor blood flow following fractionated radiotherapy in glioblastoma multiforme (GBM) due to its ability to analyze blood-brain barrier permeability as well as to visualize the characteristic abnormal vasculature [104]. Early changes in cerebral blood volume (CBV) and thus tumor perfusion following treatment were detected. In addition to visualizing changes in tumor blood flow, the technique has also been used to distinguish recurrent gliomas from radiation injury [105]. Quantitative microcirculatory values derived from pharmacokinetic modeling were significantly different in tumors, necrotic regions, and normal white matter. For example, the transfer constant between intra- and extravascular and extracellular space (K^{trans}) was significantly lower in normal white matter and highest in the recurrent glioma group. DCE-MRI may be a promising method of imaging changes in blood flow following radiation treatment as well as determining treatment efficacy with the potential to individualize and modify treatment based on early patient response [106].

Changes in tumor vascularization can also be detected through US. US contrast agents such as gas-filled microbubbles can be injected intravenously to detect a material with different acoustic properties from the tissue [107]. For example, cyanoacrylate microbubbles targeting angiogenic and inflammatory markers have been used to assess changes in tumor vascularization following radiation therapy in a preclinical prostate cancer model [108]. In addition, the dynamic contrast-enhanced (DCE)-US technique evaluates microvessel density and perfusion [109]. By utilizing sulfur hexafluoride microbubbles stabilized by a phospholipid shell, changes in vascularization following anticancer treatment, including combination radio- and chemotherapy, were observed in patients with a broad range of tumors [110]. DCE-US imaging of a patient with advanced renal cell carcinoma showed decreases in contrast uptake and thus tumor vascularity following chemotherapy treatment [111]. Many clinical trials have moved forward evaluating tumor response to chemotherapy [112-114], and future use of this technique for determining radiation response is reasonable.

PET tracers that can evaluate molecular markers of angiogenesis rather than hemodynamic characteristics, including radiolabeled arginine-glycine-aspartate (RGD) peptides, have also been used to evaluate vascular changes following treatment [115]. The most commonly used tracer for this purpose is the ^{18}F-galacto-RGD peptide that binds to $\alpha_v\beta_3$ integrins [116, 117]. Clinical trials have successfully correlated ^{18}F-galacto-RGD uptake to immunohistochemical staining of $\alpha_v\beta_3$, and have shown the feasibility of using this marker for imaging angiogenesis [118, 119]. The tracer, however, cannot distinguish between endothelial cells and tumor cells that express the integrin or between vasculature in benign and malignant lesions [116].

Future perspectives

Overall, imaging techniques that take biological considerations into account are imperative for understanding how the complex and heterogeneous tumor microenvironment influences response to therapy. Imaging biological processes from metabolism, hypoxia, proliferation, apoptosis, necrosis, and tumor vascularity enable the evaluation of the response of individual microenvironmental components directly related to therapy. Current trends focus on obtaining biological information in more detail to evaluate the underlying mechanisms of tumor structural and functional changes. Because each technique has its own limitations be it sensitivity, specificity, or patient-to-patient variation, it will likely be necessary to use complementary techniques to obtain a more balanced perspective of the response rather than using one technique or one biological process as a universal solution. In addition to determining changes in the tumor itself, assessing surrounding damage or normal tissue response is also crucial for the full evaluation of therapeutic response. Establishing early response to treatment is also a key for evaluating treatment efficacy, which has been shown in the clinic with MRSI, PET, or MRI techniques that assess metabolism, cell proliferation, apoptosis, and vascular properties.

Clinical imaging has progressed significantly from planar X-ray films to high resolution 3D functional imaging. Beyond visualizing tumor size and morphology, molecular imaging provides valuable information about the tumor microenvironment and may be used to predict and assess clinical outcomes following radiation therapy. Advances in PET, MRI, and US techniques have allowed for a deeper understanding of the biological response to treatment. A large challenge, however, lies in establishing the molecular landscape following initial treatment to assist physicians in decision making for further treatment options. Standardization of metrics for image acquisition and quantitative response assessment are also essential for realizing the full potential of molecular imaging. Progress in molecular imaging may allow for personalized medicine by designing patient-specific therapies based on accurate monitoring of patient response to treatment.

Disclosure of conflict of interest

None.

Address correspondence to: Edward E Graves, Department of Radiation Oncology, Stanford University, Stanford, CA 94305, USA. Tel: 650-723-5591; E-mail: egraves@stanford.edu

References

[1] Bradley WG. History of medical imaging. Proc Am Philos Soc 2008; 152: 349-361.
[2] Owen JB, Coia LR, Hanks GE. Recent patterns of growth in radiation therapy facilities in the United States: a patterns of care study report. Int J Radiat Oncol Biol Phys 1992; 24: 983-986.
[3] Shay JW, Roninson IB. Hallmarks of senescence in carcinogenesis and cancer therapy. Oncogene 2004; 23: 2919-2933.
[4] Moding EJ, Kastan MB, Kirsch DG. Strategies for optimizing the response of cancer and normal tissues to radiation. Nat Rev Drug Discov 2013; 12: 526-542.
[5] Wahl RL, Jacene H, Kasamon Y, Lodge MA. From RECIST to PERCIST: Evolving Considerations for PET response criteria in solid tumors. J Nucl Med 2009; 50 Suppl 1: 122S-150S.
[6] Michaelis LC, Ratain MJ. Measuring response in a post-RECIST world: from black and white to shades of grey. Nat Rev Cancer 2006; 6: 409-414.
[7] Buyse M, Thirion P, Carlson RW, Burzykowski T, Molenberghs G, Piedbois P. Relation between tumour response to first-line chemotherapy and survival in advanced colorectal cancer: a

meta-analysis. Meta-Analysis Group in Cancer. Lancet 2000; 356: 373-378.
[8] Ratain MJ. Phase II oncology trials: let's be positive. Clin Cancer Res 2005; 11: 5661-5662.
[9] Goffin J, Baral S, Tu D, Nomikos D, Seymour L. Objective responses in patients with malignant melanoma or renal cell cancer in early clinical studies do not predict regulatory approval. Clin Cancer Res 2005; 11: 5928-5934.
[10] Brindle K. New approaches for imaging tumour responses to treatment. Nat Rev Cancer 2008; 8: 94-107.
[11] Allen-Auerbach M, Weber WA. Measuring response with FDG-PET: methodological aspects. Oncologist 2009; 14: 369-377.
[12] Junttila MR, de Sauvage FJ. Influence of tumour micro-environment heterogeneity on therapeutic response. Nature 2013; 501: 346-354.
[13] Schwarz JK, Grigsby PW, Dehdashti F, Delbeke D. The role of 18F-FDG PET in assessing therapy response in cancer of the cervix and ovaries. J Nucl Med 2009; 50 Suppl 1: 64S-73S.
[14] Grigsby PW, Siegel BA, Dehdashti F, Rader J, Zoberi I. Posttherapy [18F] fluorodeoxyglucose positron emission tomography in carcinoma of the cervix: response and outcome. J Clin Oncol 2004; 22: 2167-2171.
[15] Lin LL, Yang Z, Mutic S, Miller TR, Grigsby PW. FDG-PET imaging for the assessment of physiologic volume response during radiotherapy in cervix cancer. Int J Radiat Oncol Biol Phys 2006; 65: 177-181.
[16] Schwarz JK, Siegel BA, Dehdashti F, Grigsby PW. Association of posttherapy positron emission tomography with tumor response and survival in cervical carcinoma. JAMA 2007; 298: 2289-2295.
[17] Strauss LG. Fluorine-18 deoxyglucose and false-positive results: a major problem in the diagnostics of oncological patients. Eur J Nucl Med 1996; 23: 1409-1415.
[18] Hicks RJ, Mac Manus MP, Matthews JP, Hogg A, Binns D, Rischin D, Ball DL, Peters LJ. Early FDG-PET imaging after radical radiotherapy for non-small-cell lung cancer: inflammatory changes in normal tissues correlate with tumor response and do not confound therapeutic response evaluation. Int J Radiat Oncol Biol Phys 2004; 60: 412-418.
[19] Aerts HJ, Bosmans G, van Baardwijk AA, Dekker AL, Oellers MC, Lambin P, De Ruysscher D. Stability of 18F-deoxyglucose uptake locations within tumor during radiotherapy for NSCLC: a prospective study. Int J Radiat Oncol Biol Phys 2008; 71: 1402-1407.
[20] Kong FM, Frey KA, Quint LE, Ten Haken RK, Hayman JA, Kessler M, Chetty IJ, Normolle D, Eisbruch A, Lawrence TS. A pilot study of [18F] fluorodeoxyglucose positron emission tomography scans during and after radiation-based therapy in patients with non small-cell lung cancer. J Clin Oncol 2007; 25: 3116-3123.
[21] Gillham C, Zips D, Ponisch F, Evers C, Enghardt W, Abolmaali N, Zophel K, Appold S, Holscher T, Steinbach J, Kotzerke J, Herrmann T, Baumann M. Additional PET/CT in week 5-6 of radiotherapy for patients with stage III non-small cell lung cancer as a means of dose escalation planning? Radiother Oncol 2008; 88: 335-341.
[22] Nelson SJ, Graves E, Pirzkall A, Li X, Antiniw Chan A, Vigneron DB, McKnight TR. In vivo molecular imaging for planning radiation therapy of gliomas: an application of 1H MRSI. J Magn Reson Imaging 2002; 16: 464-476.
[23] Alger JR, Frank JA, Bizzi A, Fulham MJ, DeSouza BX, Duhaney MO, Inscoe SW, Black JL, van Zijl PC, Moonen CT, et al. Metabolism of human gliomas: assessment with H-1 MR spectroscopy and F-18 fluorodeoxyglucose PET. Radiology 1990; 177: 633-641.
[24] Negendank WG, Sauter R, Brown TR, Evelhoch JL, Falini A, Gotsis ED, Heerschap A, Kamada K, Lee BC, Mengeot MM, Moser E, Padavic-Shaller KA, Sanders JA, Spraggins TA, Stillman AE, Terwey B, Vogl TJ, Wicklow K, Zimmerman RA. Proton magnetic resonance spectroscopy in patients with glial tumors: a multicenter study. J Neurosurg 1996; 84: 449-458.
[25] Preul MC, Caramanos Z, Collins DL, Villemure JG, Leblanc R, Olivier A, Pokrupa R, Arnold DL. Accurate, noninvasive diagnosis of human brain tumors by using proton magnetic resonance spectroscopy. Nat Med 1996; 2: 323-325.
[26] Graves EE, Nelson SJ, Vigneron DB, Chin C, Verhey L, McDermott M, Larson D, Sneed PK, Chang S, Prados MD, Lamborn K, Dillon WP. A preliminary study of the prognostic value of proton magnetic resonance spectroscopic imaging in gamma knife radiosurgery of recurrent malignant gliomas. Neurosurgery 2000; 46: 319-326; discussion 326-318.
[27] Graves EE, Nelson SJ, Vigneron DB, Verhey L, McDermott M, Larson D, Chang S, Prados MD, Dillon WP. Serial proton MR spectroscopic imaging of recurrent malignant gliomas after gamma knife radiosurgery. AJNR Am J Neuroradiol 2001; 22: 613-624.
[28] Brindle K. Watching tumours gasp and die with MRI: the promise of hyperpolarised 13C MR spectroscopic imaging. Br J Radiol 2012; 85: 697-708.
[29] Day SE, Kettunen MI, Gallagher FA, Hu DE, Lerche M, Wolber J, Golman K, Ardenkjaer-Larsen JH, Brindle KM. Detecting tumor re-

sponse to treatment using hyperpolarized 13C magnetic resonance imaging and spectroscopy. Nat Med 2007; 13: 1382-1387.
[30] Gallagher FA, Kettunen MI, Hu DE, Jensen PR, Zandt RI, Karlsson M, Gisselsson A, Nelson SK, Witney TH, Bohndiek SE, Hansson G, Peitersen T, Lerche MH, Brindle KM. Production of hyperpolarized [1, 4-13C2] malate from [1, 4-13C2] fumarate is a marker of cell necrosis and treatment response in tumors. Proc Natl Acad Sci U S A 2009; 106: 19801-19806.
[31] Qu W, Zha Z, Lieberman BP, Mancuso A, Stetz M, Rizzi R, Ploessl K, Wise D, Thompson C, Kung HF. Facile synthesis [5-(13) C-4-(2) H (2)]-L-glutamine for hyperpolarized MRS imaging of cancer cell metabolism. Acad Radiol 2011; 18: 932-939.
[32] Nelson SJ, Kurhanewicz J, Vigneron DB, Larson PE, Harzstark AL, Ferrone M, van Criekinge M, Chang JW, Bok R, Park I, Reed G, Carvajal L, Small EJ, Munster P, Weinberg VK, Ardenkjaer-Larsen JH, Chen AP, Hurd RE, Odegardstuen LI, Robb FJ, Tropp J, Murray JA. Metabolic imaging of patients with prostate cancer using hyperpolarized [1-(1) (3) C]pyruvate. Sci Transl Med 2013; 5: 198ra108.
[33] Tatum JL, Kelloff GJ, Gillies RJ, Arbeit JM, Brown JM, Chao KS, Chapman JD, Eckelman WC, Fyles AW, Giaccia AJ, Hill RP, Koch CJ, Krishna MC, Krohn KA, Lewis JS, Mason RP, Melillo G, Padhani AR, Powis G, Rajendran JG, Reba R, Robinson SP, Semenza GL, Swartz HM, Vaupel P, Yang D, Croft B, Hoffman J, Liu G, Stone H, Sullivan D. Hypoxia: importance in tumor biology, noninvasive measurement by imaging, and value of its measurement in the management of cancer therapy. Int J Radiat Biol 2006; 82: 699-757.
[34] Wilson WR, Hay MP. Targeting hypoxia in cancer therapy. Nat Rev Cancer 2011; 11: 393-410.
[35] Mees G, Dierckx R, Vangestel C, Van de Wiele C. Molecular imaging of hypoxia with radiolabelled agents. Eur J Nucl Med Mol Imaging 2009; 36: 1674-1686.
[36] Koh WJ, Rasey JS, Evans ML, Grierson JR, Lewellen TK, Graham MM, Krohn KA, Griffin TW. Imaging of hypoxia in human tumors with [F-18] fluoromisonidazole. Int J Radiat Oncol Biol Phys 1992; 22: 199-212.
[37] Lee ST, Scott AM. Hypoxia positron emission tomography imaging with 18f-fluoromisonidazole. Semin Nucl Med 2007; 37: 451-461.
[38] Komar G, Seppanen M, Eskola O, Lindholm P, Gronroos TJ, Forsback S, Sipila H, Evans SM, Solin O, Minn H. 18F-EF5: a new PET tracer for imaging hypoxia in head and neck cancer. J Nucl Med 2008; 49: 1944-1951.
[39] Eschmann SM, Paulsen F, Reimold M, Dittmann H, Welz S, Reischl G, Machulla HJ, Bares R. Prognostic impact of hypoxia imaging with 18F-misonidazole PET in non-small cell lung cancer and head and neck cancer before radiotherapy. J Nucl Med 2005; 46: 253-260.
[40] Souvatzoglou M, Grosu AL, Roper B, Krause BJ, Beck R, Reischl G, Picchio M, Machulla HJ, Wester HJ, Piert M. Tumour hypoxia imaging with [18F] FAZA PET in head and neck cancer patients: a pilot study. Eur J Nucl Med Mol Imaging 2007; 34: 1566-1575.
[41] Rasey JS, Koh WJ, Evans ML, Peterson LM, Lewellen TK, Graham MM, Krohn KA. Quantifying regional hypoxia in human tumors with positron emission tomography of [18F] fluoromisonidazole: a pretherapy study of 37 patients. Int J Radiat Oncol Biol Phys 1996; 36: 417-428.
[42] Krohn KA, Link JM, Mason RP. Molecular imaging of hypoxia. J Nucl Med 2008; 49 Suppl 2: 129S-148S.
[43] Carlin S, Humm JL. PET of hypoxia: current and future perspectives. J Nucl Med 2012; 53: 1171-1174.
[44] Eschmann SM, Paulsen F, Bedeshem C, Machulla HJ, Hehr T, Bamberg M, Bares R. Hypoxia-imaging with (18) F-Misonidazole and PET: changes of kinetics during radiotherapy of head-and-neck cancer. Radiother Oncol 2007; 83: 406-410.
[45] Tachibana I, Nishimura Y, Shibata T, Kanamori S, Nakamatsu K, Koike R, Nishikawa T, Ishikawa K, Tamura M, Hosono M. A prospective clinical trial of tumor hypoxia imaging with 18F-fluoromisonidazole positron emission tomography and computed tomography (F-MISO PET/CT) before and during radiation therapy. J Radiat Res 2013; 54: 1078-1084.
[46] Rajendran JG, Wilson DC, Conrad EU, Peterson LM, Bruckner JD, Rasey JS, Chin LK, Hofstrand PD, Grierson JR, Eary JF, Krohn KA. [(18) F] FMISO and [(18) F] FDG PET imaging in soft tissue sarcomas: correlation of hypoxia, metabolism and VEGF expression. Eur J Nucl Med Mol Imaging 2003; 30: 695-704.
[47] Cherk MH, Foo SS, Poon AM, Knight SR, Murone C, Papenfuss AT, Sachinidis JI, Saunder TH, O'Keefe GJ, Scott AM. Lack of correlation of hypoxic cell fraction and angiogenesis with glucose metabolic rate in non-small cell lung cancer assessed by 18F-Fluoromisonidazole and 18F-FDG PET. J Nucl Med 2006; 47: 1921-1926.
[48] Mortensen LS, Busk M, Nordsmark M, Jakobsen S, Theil J, Overgaard J, Horsman MR. Accessing radiation response using hypoxia PET imaging and oxygen sensitive electrodes: a preclinical study. Radiother Oncol 2011; 99: 418-423.
[49] Postema EJ, McEwan AJ, Riauka TA, Kumar P, Richmond DA, Abrams DN, Wiebe LI. Initial re-

sults of hypoxia imaging using 1-alpha-D: -(5-deoxy-5-[18F]-fluoroarabinofuranosyl)-2-nitroimidazole (18F-FAZA). Eur J Nucl Med Mol Imaging 2009; 36: 1565-1573.
[50] Trinkaus ME, Blum R, Rischin D, Callahan J, Bressel M, Segard T, Roselt P, Eu P, Binns D, MacManus MP, Ball D, Hicks RJ. Imaging of hypoxia with 18F-FAZA PET in patients with locally advanced non-small cell lung cancer treated with definitive chemoradiotherapy. J Med Imaging Radiat Oncol 2013; 57: 475-481.
[51] Dehdashti F, Grigsby PW, Mintun MA, Lewis JS, Siegel BA, Welch MJ. Assessing tumor hypoxia in cervical cancer by positron emission tomography with 60Cu-ATSM: relationship to therapeutic response-a preliminary report. Int J Radiat Oncol Biol Phys 2003; 55: 1233-1238.
[52] Dehdashti F, Mintun MA, Lewis JS, Bradley J, Govindan R, Laforest R, Welch MJ, Siegel BA. In vivo assessment of tumor hypoxia in lung cancer with 60Cu-ATSM. Eur J Nucl Med Mol Imaging 2003; 30: 844-850.
[53] O'Donoghue JA, Zanzonico P, Pugachev A, Wen B, Smith-Jones P, Cai S, Burnazi E, Finn RD, Burgman P, Ruan S, Lewis JS, Welch MJ, Ling CC, Humm JL. Assessment of regional tumor hypoxia using 18F-fluoromisonidazole and 64Cu (II)-diacetyl-bis (N4-methylthiosemicarbazone) positron emission tomography: Comparative study featuring microPET imaging, Po2 probe measurement, autoradiography, and fluorescent microscopy in the R3327-AT and FaDu rat tumor models. Int J Radiat Oncol Biol Phys 2005; 61: 1493-1502.
[54] Yuan H, Schroeder T, Bowsher JE, Hedlund LW, Wong T, Dewhirst MW. Intertumoral differences in hypoxia selectivity of the PET imaging agent 64Cu (II)-diacetyl-bis (N4-methylthiosemicarbazone). J Nucl Med 2006; 47: 989-998.
[55] Taylor NJ, Baddeley H, Goodchild KA, Powell ME, Thoumine M, Culver LA, Stirling JJ, Saunders MI, Hoskin PJ, Phillips H, Padhani AR, Griffiths JR. BOLD MRI of human tumor oxygenation during carbogen breathing. J Magn Reson Imaging 2001; 14: 156-163.
[56] Hallac RR, Ding Y, Yuan Q, McColl RW, Lea J, Sims RD, Weatherall PT, Mason RP. Oxygenation in cervical cancer and normal uterine cervix assessed using blood oxygenation level-dependent (BOLD) MRI at 3T. NMR Biomed 2012; 25: 1321-1330.
[57] Lee CT, Boss MK, Dewhirst MW. Imaging tumor hypoxia to advance radiation oncology. Antioxid Redox Signal 2014; 21: 313-337.
[58] Kim CK, Park SY, Park BK, Park W, Huh SJ. Blood oxygenation level-dependent MR imaging as a predictor of therapeutic response to concurrent chemoradiotherapy in cervical cancer: a preliminary experience. Eur Radiol 2014; 24: 1514-1520.
[59] Baudelet C, Gallez B. How does blood oxygen level-dependent (BOLD) contrast correlate with oxygen partial pressure (pO2) inside tumors? Magn Reson Med 2002; 48: 980-986.
[60] Hallac RR, Zhou H, Pidikiti R, Song K, Stojadinovic S, Zhao D, Solberg T, Peschke P, Mason RP. Correlations of noninvasive BOLD and TOLD MRI with pO2 and relevance to tumor radiation response. Magn Reson Med 2014; 71: 1863-1873.
[61] Boothman DA, Davis TW, Sahijdak WM. Enhanced expression of thymidine kinase in human cells following ionizing radiation. Int J Radiat Oncol Biol Phys 1994; 30: 391-398.
[62] Been LB, Suurmeijer AJ, Cobben DC, Jager PL, Hoekstra HJ, Elsinga PH. [18F]FLT-PET in oncology: current status and opportunities. Eur J Nucl Med Mol Imaging 2004; 31: 1659-1672.
[63] Hoeben BA, Troost EG, Span PN, van Herpen CM, Bussink J, Oyen WJ, Kaanders JH. 18F-FLT PET during radiotherapy or chemoradiotherapy in head and neck squamous cell carcinoma is an early predictor of outcome. J Nucl Med 2013; 54: 532-540.
[64] Everitt S, Hicks RJ, Ball D, Kron T, Schneider-Kolsky M, Walter T, Binns D, Mac Manus M. Imaging cellular proliferation during chemo-radiotherapy: a pilot study of serial 18F-FLT positron emission tomography/computed tomography imaging for non-small-cell lung cancer. Int J Radiat Oncol Biol Phys 2009; 75: 1098-1104.
[65] Everitt SJ, Ball DL, Hicks RJ, Callahan J, Plumridge N, Collins M, Herschtal A, Binns D, Kron T, Schneider M, MacManus M. Differential 18F-FDG and 18F-FLT Uptake on Serial PET/CT Imaging Before and During Definitive Chemoradiation for Non-Small Cell Lung Cancer. J Nucl Med 2014; 55: 1069-1074.
[66] McKinley ET, Ayers GD, Smith RA, Saleh SA, Zhao P, Washington MK, Coffey RJ, Manning HC. Limits of [18F]-FLT PET as a biomarker of proliferation in oncology. PLoS One 2013; 8: e58938.
[67] Mach RH, Dehdashti F, Wheeler KT. PET Radiotracers for Imaging the Proliferative Status of Solid Tumors. PET Clin 2009; 4: 1-15.
[68] Xu J, Zeng C, Chu W, Pan F, Rothfuss JM, Zhang F, Tu Z, Zhou D, Zeng D, Vangveravong S, Johnston F, Spitzer D, Chang KC, Hotchkiss RS, Hawkins WG, Wheeler KT, Mach RH. Identification of the PGRMC1 protein complex as the putative sigma-2 receptor binding site. Nat Commun 2011; 2: 380.
[69] Dehdashti F, Laforest R, Gao F, Shoghi KI, Aft RL, Nussenbaum B, Kreisel FH, Bartlett NL, Cashen A, Wagner-Johnston N, Mach RH.

Assessment of cellular proliferation in tumors by PET using 18F-ISO-1. J Nucl Med 2013; 54: 350-357.
[70] Shoghi KI, Xu J, Su Y, He J, Rowland D, Yan Y, Garbow JR, Tu Z, Jones LA, Higashikubo R, Wheeler KT, Lubet RA, Mach RH, You M. Quantitative receptor-based imaging of tumor proliferation with the sigma-2 ligand [(18)F] ISO-1. PLoS One 2013; 8: e74188.
[71] Hanahan D, Weinberg RA. The hallmarks of cancer. Cell 2000; 100: 57-70.
[72] Stephens LC, Hunter NR, Ang KK, Milas L, Meyn RE. Development of apoptosis in irradiated murine tumors as a function of time and dose. Radiat Res 1993; 135: 75-80.
[73] Dewey WC, Ling CC, Meyn RE. Radiation-induced apoptosis: relevance to radiotherapy. Int J Radiat Oncol Biol Phys 1995; 33: 781-796.
[74] Brown JM, Attardi LD. The role of apoptosis in cancer development and treatment response. Nat Rev Cancer 2005; 5: 231-237.
[75] Pinar B, Henriquez-Hernandez LA, Lara PC, Bordon E, Rodriguez-Gallego C, Lloret M, Nunez MI, De Almodovar MR. Radiation induced apoptosis and initial DNA damage are inversely related in locally advanced breast cancer patients. Radiat Oncol 2010; 5: 85.
[76] Huang Q, Li F, Liu X, Li W, Shi W, Liu FF, O'Sullivan B, He Z, Peng Y, Tan AC, Zhou L, Shen J, Han G, Wang XJ, Thorburn J, Thorburn A, Jimeno A, Raben D, Bedford JS, Li CY. Caspase 3-mediated stimulation of tumor cell repopulation during cancer radiotherapy. Nat Med 2011; 17: 860-866.
[77] Hu W, Kavanagh JJ. Anticancer therapy targeting the apoptotic pathway. Lancet Oncol 2003; 4: 721-729.
[78] Meiler J, Schuler M. Therapeutic targeting of apoptotic pathways in cancer. Curr Drug Targets 2006; 7: 1361-1369.
[79] Fernandez-Luna JL. Apoptosis regulators as targets for cancer therapy. Clin Transl Oncol 2007; 9: 555-562.
[80] Maddika S, Ande SR, Panigrahi S, Paranjothy T, Weglarczyk K, Zuse A, Eshraghi M, Manda KD, Wiechec E, Los M. Cell survival, cell death and cell cycle pathways are interconnected: implications for cancer therapy. Drug Resist Updat 2007; 10: 13-29.
[81] Call JA, Eckhardt SG, Camidge DR. Targeted manipulation of apoptosis in cancer treatment. Lancet Oncol 2008; 9: 1002-1011.
[82] Meyn RE, Milas L, Ang KK. The role of apoptosis in radiation oncology. Int J Radiat Biol 2009; 85: 107-115.
[83] Porter AG, Janicke RU. Emerging roles of caspase-3 in apoptosis. Cell Death Differ 1999; 6: 99-104.
[84] Smith G, Glaser M, Perumal M, Nguyen QD, Shan B, Arstad E, Aboagye EO. Design, synthesis, and biological characterization of a caspase 3/7 selective isatin labeled with 2-[18F] fluoroethylazide. J Med Chem 2008; 51: 8057-8067.
[85] Nguyen QD, Smith G, Glaser M, Perumal M, Arstad E, Aboagye EO. Positron emission tomography imaging of drug-induced tumor apoptosis with a caspase-3/7 specific [18F]-labeled isatin sulfonamide. Proc Natl Acad Sci U S A 2009; 106: 16375-16380.
[86] Nguyen QD, Challapalli A, Smith G, Fortt R, Aboagye EO. Imaging apoptosis with positron emission tomography: 'bench to bedside' development of the caspase-3/7 specific radiotracer [(18)F]ICMT-11. Eur J Cancer 2012; 48: 432-440.
[87] Challapalli A, Kenny LM, Hallett WA, Kozlowski K, Tomasi G, Gudi M, Al-Nahhas A, Coombes RC, Aboagye EO. 18F-ICMT-11, a caspase-3-specific PET tracer for apoptosis: biodistribution and radiation dosimetry. J Nucl Med 2013; 54: 1551-1556.
[88] Lee D, Long SA, Murray JH, Adams JL, Nuttall ME, Nadeau DP, Kikly K, Winkler JD, Sung CM, Ryan MD, Levy MA, Keller PM, DeWolf WE, Jr. Potent and selective nonpeptide inhibitors of caspases 3 and 7. J Med Chem 2001; 44: 2015-2026.
[89] Reshef A, Shirvan A, Akselrod-Ballin A, Wall A, Ziv I. Small-molecule biomarkers for clinical PET imaging of apoptosis. J Nucl Med 2010; 51: 837-840.
[90] Allen AM, Ben-Ami M, Reshef A, Steinmetz A, Kundel Y, Inbar E, Djaldetti R, Davidson T, Fenig E, Ziv I. Assessment of response of brain metastases to radiotherapy by PET imaging of apoptosis with $^{(18)}$F-ML-10. Eur J Nucl Med Mol Imaging 2012; 39: 1400-1408.
[91] Cohen A, Shirvan A, Levin G, Grimberg H, Reshef A, Ziv I. From the Gla domain to a novel small-molecule detector of apoptosis. Cell Res 2009; 19: 625-637.
[92] Jain R, Narang J, Sundgren PM, Hearshen D, Saksena S, Rock JP, Gutierrez J, Mikkelsen T. Treatment induced necrosis versus recurrent/progressing brain tumor: going beyond the boundaries of conventional morphologic imaging. J Neurooncol 2010; 100: 17-29.
[93] Mullins ME, Barest GD, Schaefer PW, Hochberg FH, Gonzalez RG, Lev MH. Radiation necrosis versus glioma recurrence: conventional MR imaging clues to diagnosis. AJNR Am J Neuroradiol 2005; 26: 1967-1972.
[94] Zhou J, Payen JF, Wilson DA, Traystman RJ, van Zijl PC. Using the amide proton signals of intracellular proteins and peptides to detect pH effects in MRI. Nat Med 2003; 9: 1085-1090.

[95] Zhou J, Tryggestad E, Wen Z, Lal B, Zhou T, Grossman R, Wang S, Yan K, Fu DX, Ford E, Tyler B, Blakeley J, Laterra J, van Zijl PC. Differentiation between glioma and radiation necrosis using molecular magnetic resonance imaging of endogenous proteins and peptides. Nat Med 2011; 17: 130-134.

[96] Zhang H, Ma L, Shu C, Wang Y, Dong L. Diagnostic accuracy of diffusion MRI with quantitative ADC measurements in differentiating glioma recurrence from radiation necrosis. J Neurol Sci 2015; 351: 65-71.

[97] Wang HZ, Qiu SJ, Lv XF, Wang YY, Liang Y, Xiong WF, Ouyang ZB. Diffusion tensor imaging and 1H-MRS study on radiation-induced brain injury after nasopharyngeal carcinoma radiotherapy. Clin Radiol 2012; 67: 340-345.

[98] Carmeliet P, Jain RK. Principles and mechanisms of vessel normalization for cancer and other angiogenic diseases. Nat Rev Drug Discov 2011; 10: 417-427.

[99] Zahra MA, Hollingsworth KG, Sala E, Lomas DJ, Tan LT. Dynamic contrast-enhanced MRI as a predictor of tumour response to radiotherapy. Lancet Oncol 2007; 8: 63-74.

[100] Boucher Y, Baxter LT, Jain RK. Interstitial pressure gradients in tissue-isolated and subcutaneous tumors: implications for therapy. Cancer Res 1990; 50: 4478-4484.

[101] Gerlowski LE, Jain RK. Microvascular permeability of normal and neoplastic tissues. Microvasc Res 1986; 31: 288-305.

[102] de Lussanet QG, Backes WH, Griffioen AW, Padhani AR, Baeten CI, van Baardwijk A, Lambin P, Beets GL, van Engelshoven JM, Beets-Tan RG. Dynamic contrast-enhanced magnetic resonance imaging of radiation therapy-induced microcirculation changes in rectal cancer. Int J Radiat Oncol Biol Phys 2005; 63: 1309-1315.

[103] Cao Y, Popovtzer A, Li D, Chepeha DB, Moyer JS, Prince ME, Worden F, Teknos T, Bradford C, Mukherji SK, Eisbruch A. Early prediction of outcome in advanced head-and-neck cancer based on tumor blood volume alterations during therapy: a prospective study. Int J Radiat Oncol Biol Phys 2008; 72: 1287-1290.

[104] Cao Y, Tsien CI, Nagesh V, Junck L, Ten Haken R, Ross BD, Chenevert TL, Lawrence TS. Survival prediction in high-grade gliomas by MRI perfusion before and during early stage of RT [corrected]. Int J Radiat Oncol Biol Phys 2006; 64: 876-885.

[105] Bisdas S, Naegele T, Ritz R, Dimostheni A, Pfannenberg C, Reimold M, Koh TS, Ernemann U. Distinguishing recurrent high-grade gliomas from radiation injury: a pilot study using dynamic contrast-enhanced MR imaging. Acad Radiol 2011; 18: 575-583.

[106] Cao Y. The promise of dynamic contrast-enhanced imaging in radiation therapy. Semin Radiat Oncol 2011; 21: 147-156.

[107] Blomley MJ, Cooke JC, Unger EC, Monaghan MJ, Cosgrove DO. Microbubble contrast agents: a new era in ultrasound. BMJ 2001; 322: 1222-1225.

[108] Palmowski M, Peschke P, Huppert J, Hauff P, Reinhardt M, Maurer M, Karger CP, Scholz M, Semmler W, Huber PE, Kiessling FM. Molecular ultrasound imaging of early vascular response in prostate tumors irradiated with carbon ions. Neoplasia 2009; 11: 856-863.

[109] Hwang M, Niermann KJ, Lyshchik A, Fleischer AC. Sonographic assessment of tumor response: from in vivo models to clinical applications. Ultrasound Q 2009; 25: 175-183.

[110] Lassau N, Chami L, Benatsou B, Peronneau P, Roche A. Dynamic contrast-enhanced ultrasonography (DCE-US) with quantification of tumor perfusion: a new diagnostic tool to evaluate the early effects of antiangiogenic treatment. Eur Radiol 2007; 17 Suppl 6: F89-98.

[111] Escudier B, Lassau N, Angevin E, Soria JC, Chami L, Lamuraglia M, Zafarana E, Landreau V, Schwartz B, Brendel E, Armand JP, Robert C. Phase I trial of sorafenib in combination with IFN alpha-2a in patients with unresectable and/or metastatic renal cell carcinoma or malignant melanoma. Clin Cancer Res 2007; 13: 1801-1809.

[112] De Giorgi U, Aliberti C, Benea G, Conti M, Marangolo M. Effect of angiosonography to monitor response during imatinib treatment in patients with metastatic gastrointestinal stromal tumors. Clin Cancer Res 2005; 11: 6171-6176.

[113] Lassau N, Chami L, Peronneau P. [Imaging of melanoma: accuracy of ultrasonography before and after contrast injection for diagnostic and early evaluation of treatments]. Bull Cancer 2007; 94: 93-98.

[114] Lassau N, Lamuraglia M, Chami L, Leclere J, Bonvalot S, Terrier P, Roche A, Le Cesne A. Gastrointestinal stromal tumors treated with imatinib: monitoring response with contrast-enhanced sonography. AJR Am J Roentgenol 2006; 187: 1267-1273.

[115] Gaertner FC, Kessler H, Wester HJ, Schwaiger M, Beer AJ. Radiolabelled RGD peptides for imaging and therapy. Eur J Nucl Med Mol Imaging 2012; 39 Suppl 1: S126-138.

[116] Haubner R, Weber WA, Beer AJ, Vabuliene E, Reim D, Sarbia M, Becker KF, Goebel M, Hein R, Wester HJ, Kessler H, Schwaiger M. Noninvasive visualization of the activated alphavbeta3 integrin in cancer patients by positron emission tomography and [18F]Galacto-RGD. PLoS Med 2005; 2: e70.

[117] Beer AJ, Haubner R, Goebel M, Luderschmidt S, Spilker ME, Wester HJ, Weber WA, Schwaiger M. Biodistribution and pharmacokinetics of the alphavbeta3-selective tracer 18F-galacto-RGD in cancer patients. J Nucl Med 2005; 46: 1333-1341.

[118] Haubner R, Kuhnast B, Mang C, Weber WA, Kessler H, Wester HJ, Schwaiger M. [18F] Galacto-RGD: synthesis, radiolabeling, metabolic stability, and radiation dose estimates. Bioconjug Chem 2004; 15: 61-69.

[119] Beer AJ, Haubner R, Sarbia M, Goebel M, Luderschmidt S, Grosu AL, Schnell O, Niemeyer M, Kessler H, Wester HJ, Weber WA, Schwaiger M. Positron emission tomography using [18F] Galacto-RGD identifies the level of integrin alpha(v) beta3 expression in man. Clin Cancer Res 2006; 12: 3942-3949.